


Comparison of mitochondrial genomes provides insights into intron dynamics and evolution in *Botryosphaeria dothidea* and *B. kuwatsukai*

Bo Wang ^{1,2} Xiaofei Liang,¹ Xiaojuan Hao,¹ Haiyue Dang,¹ Tom Hsiang,³ Mark L. Gleason,⁴ Rong Zhang¹ and Guangyu Sun ^{1*}

¹State Key Laboratory of Crop Stress Biology in Arid Areas and College of Plant Protection, Northwest A&F University, Yangling, Shaanxi, 712100, China.

²MOE Key Laboratory for Intelligent Networks & Network Security, Faculty of Electronic and Information Engineering, Xi'an Jiaotong University, Xi'an, 710049, China.

³School of Environmental Sciences, University of Guelph, Guelph, ON, N1G 2W1, Canada.

⁴Department of Plant Pathology and Microbiology, Iowa State University, Ames, IA, 50011.

Summary

Botryosphaeria dothidea is one of the most common fungal pathogens on a large number of hosts worldwide. *Botryosphaeria dothidea* and *B. kuwatsukai* are also the main causal agents of apple ring rot. In this study, we sequenced, assembled and annotated the circular mitogenomes of 12 diverse *B. dothidea* isolates (105.7–114.8 kb) infecting various plants including apple, and five diverse *B. kuwatsukai* isolates (118.0–124.6 kb) from apple. *B. dothidea* mitogenomes harboured a set of 29–31 introns and 48–52 ORFs. In contrast, *B. kuwatsukai* mitogenomes harboured more introns (32–34) and ORFs (51–54). The variation in mitogenome sizes was associated mainly with different numbers of introns and insertions of mobile genetic elements. Interestingly, *B. dothidea* and *B. kuwatsukai* displayed distinct intron distribution patterns, with three intron loci showing presence/absence dynamics in each species. Large numbers of introns (57% in *B. dothidea* and 49% in *B. kuwatsukai*) were most likely obtained through horizontal transfer from non-Dothideomycetes. The mitochondrial gene

phylogeny supported the differentiation of the two species. Overall, this study sheds light into the mitochondrial evolution of the plant pathogens *B. dothidea* and *B. kuwatsukai*, and intron distribution patterns could be useful markers for studies on population diversity.

Introduction

Fungi in the family Botryosphaeriaceae are among the most cosmopolitan fungi, and many species in this family are important canker and dieback pathogens of woody plants worldwide. *Botryosphaeria dothidea* is one of the most prominent pathogens on a large number of hosts, including more than 24 host genera, with 285 records in the literature, causing many destructive diseases, such as poplar canker, grape branch blight and apple ring rot (Marsberg *et al.*, 2017). Ring rot, caused by *B. dothidea* and *B. kuwatsukai*, is one of the most destructive apple diseases worldwide, including China, Japan, South Korea, the United States, Australia and South Africa (Xu *et al.*, 2015). Ring rot symptoms of the disease include a soft, light-coloured rot on fruit, especially during storage, and extensive cankers or warts on branches and trunks (Chen, 1999). Xu *et al.* (2015) reappraised the aetiology of apple ring rot and considered *B. kuwatsukai* and *B. dothidea* to be the main causal agents in China.

Botryosphaeria kuwatsukai demonstrated substantial genetic and biological distinctions from *B. dothidea*. For example, the two species possess different intron insertion positions in the primary structures of the rDNA SSU (Xu *et al.*, 2013, 2015). Morphologically, *B. kuwatsukai* presents aerial mycelium compact on potato dextrose agar (PDA), whereas *B. dothidea* displays funicle of aerial mycelium well developed of the Petri plates. Conidia of *B. kuwatsukai* are longer than those of *B. dothidea*, whereas *B. dothidea* has a faster growth rate than *B. kuwatsukai* at 35°C and 37°C (Xu *et al.*, 2015). Pathogenicity tests showed that *B. kuwatsukai* caused large cankers and bark blisters on pear (*Pyrus communis*), whereas *B. dothidea* was non-pathogenic on pear; however, on apple shoots, *B. kuwatsukai* and *B. dothidea*

Received 24 March, 2021; revised 18 May, 2021; accepted 19 May, 2021. *For correspondence. E-mail sgy@nwsuaf.edu.cn; Tel. 86-29-87092075.

induced large and small wart-like bark swellings respectively (Xu *et al.*, 2015). The host range of *B. kuwatsukai* is apparently narrower; it has been reported only from apple and pear, whereas *B. dothidea* is able to infect a wide range of hosts (Xu *et al.*, 2015).

In a previous study, we sequenced the nuclear genomes of *B. dothidea* and *B. kuwatsukai*, and conducted a genomic level comparative analysis of these two genomes (Wang *et al.*, 2018a). We found that *B. kuwatsukai*, compared to *B. dothidea*, apparently lost a set of carbohydrate-active enzymes, plant cell wall-degrading enzymes and secondary metabolites biosynthetic enzymes, possibly as a result of host specialization (Wang *et al.*, 2018a).

Mitogenomes are a valuable source of genetic information and have been successfully used in evolutionary biology and systematic studies in eukaryotes (Pantou *et al.*, 2006; Kouvelis *et al.*, 2008). Mitochondrial genes evolve more quickly than nuclear genes (Ballard and Whitlock, 2004), but for yeast, the opposite is true (De Chiara *et al.*, 2020). Fungal mitogenomes are characterized by a variable number of group I and group II introns that may carry homing endonuclease genes (HEGs) with LAGLIDADG or GIY-YIG motifs (Lang *et al.*, 1999; Bullerwell and Lang, 2005; Lang *et al.*, 2007). In general, group I introns are abundant in fungal mitogenomes, while group II introns are predominant in plant mitogenomes. Group I introns are further divided into several subgroups (e.g. IA, IA3, IB, IC1, IC2, ID) based on phylogenetic analyses. Occurrence of these subgroups is uneven among fungi, with subgroup IB being generally more frequent than other subgroups (Lang *et al.*, 2007). Recently, mitochondrial genomes have been widely used for phylogenetic analysis in plant, animals and fungi (Shen *et al.*, 2015; Li *et al.*, 2019; Hu *et al.*, 2020; Yang *et al.*, 2021).

HEGs are selfish genetic mobile elements that encode endonucleases whose catalytic activity promotes their own propagation by introducing DNA double-strand breaks (DSBs) into alleles lacking the endonuclease-coding sequence, and by the subsequent repair of these DSBs via homologous recombination using the endonuclease-containing allele as template (Burt and Koufopanou, 2004; Edgell, 2009). This mechanism of propagation can result in the insertion, deletion or mutation of DNA sequences (Stoddard, 2011). Indeed, mobile introns and HEGs represent one of the major sources of variability within fungal mitogenomes (Repar and Warnecke, 2017).

In this study, we assembled and annotated mitogenomes of 12 *B. dothidea* isolates recovered from several hosts, and five *B. kuwatsukai* isolates from apple. We compared these 17 mitogenomes in detail regarding their sizes, gene contents and arrangement, and intron characteristics. Our goals were as follows: (i) determine intraspecific

mitogenomic variations within *B. dothidea* and *B. kuwatsukai*; (ii) to investigate interspecific mitogenomic variation between the two species for speciation; and (iii) to elucidate the origin and evolution of mitochondrial introns in *Botryosphaeria* fungal species. These results should enrich the available genomic information about these two main causal agents of apple ring rot and provide valuable reference for further investigation of mitogenomic evolution in Botryosphaeriales and related species.

Materials and methods

Fungal culture conditions and identification

All fungi were single-spore cultures maintained (Table 1) on PDA medium at 25°C (Sun and Zhang, 1996), and stored in 15% glycerol at –80°C in the Fungal Laboratory of Northwest A&F University, Yangling, Shaanxi Province, China. The isolates were identified based on morphology and phylogenetic analysis. The internal transcribed spacer (ITS) and EF-1 α (translation elongation factor-1 alpha) sequences were obtained with conserved primers by PCR amplification (Bio-Rad C1000, Bio-Rad Laboratories, USA) (White *et al.*, 1990; Inderbitzin *et al.*, 2010; Xu *et al.*, 2015). The sequences of selected *B. dothidea* and *B. kuwatsukai* species were edited/assembled by BioEdit v. 7.0.9 (Hall, 1999) and uploaded to GenBank (Table S1). A maximum-likelihood phylogenetic tree based on concatenated sequences (ITS and EF-1 α) was constructed using MEGA v. 7 with the Kimura 2-parameter model (Kumar *et al.*, 2016). Statistical support for phylogenetic grouping was assessed by 1000 bootstrap re-samplings.

Genome sequencing and assembly

For isolates confirmed as *Botryosphaeria*, highly purified total genomic DNA was isolated from the fungal mycelia collected from each 2-week-old culture on PDA plate following a modified cetyltrimethylammonium bromide protocol (Murray and Thompson, 1980). The genomes were sequenced on the Illumina HiSeq™4000 platform at the Novogene Genomic Sequencing Center, Beijing, China, targeting >100 \times coverage per genome. The insertion size of the sequencing library was 350 bp with a 150 bp paired-end sequencing strategy. Reads were filtered by using fastp software (Chen *et al.*, 2018). Filtered clean reads were assembled into scaffolds using the SPAdes v. 3.9.0 with ‘--careful’ (Bankevich *et al.*, 2012). To find assemblies with the highest N50 values, SPAdes was run at multiple kmers (21, 33, 55, 77, 99). Contigs representing mitochondrial DNA sequences were identified by BLAST search against the mitogenome of *Zymoseptoria tritici* (GenBank accession: EU090238)

Table 1. Mitogenome feature of *B. dothidea* and *B. kuwatsukai* isolates used in this study.

	Isolation source	Host species	Host family	Accession no.	Mitogenome size (bp)	GC content (%)	No. introns	Introns (bp/%) ^a	No. intronic ORFs	Intergenic regions (bp/%) ^a	No. intergenic ORFs	
<i>B. dothidea</i> isolates												
PGZH20	Zhengzhou city, Henan	<i>Malus domestica</i>	Rosaceae	MG593783	105 788	29.5	29	49 858/47.1	36	31 837/30.1	12	
PGZH16	Zhengzhou city, Henan	<i>Malus domestica</i>	Rosaceae	MG593781	105 700	29.4	29	49 921/47.2	36	31 775/30.1	12	
PGLWX	Yangling city, Shaanxi	<i>Malus domestica</i>	Rosaceae	MG593778	108 247	29.6	30	52 378/48.4	38	31 777/29.4	12	
PGLB9	Lingbao city, Henan	<i>Malus domestica</i>	Rosaceae	MG593776	108 200	29.6	30	52 448/48.5	37	31 660/29.3	12	
PG45	Yangling city, Shaanxi	<i>Malus domestica</i>	Rosaceae	KY801668	109 776	29.7	31	53 998/49.2	38	31 684/28.9	12	
TCPTT1	Tongchuan city, Shaanxi	<i>Vitis vinifera</i>	Vitaceae	MT166295	114 832	29.6	31	54 175/47.2	38	35 928/31.3	14	
TS-2	Baishui city, Shaanxi	<i>Amygdalus persica</i>	Rosaceae	MT166296	108 411	29.7	30	52 502/48.4	38	31 817/29.3	12	
2g	Liquan city, Shaanxi	<i>Diospyros kaki</i>	Ebenaceae	MT166291	108 404	29.7	30	52 378/48.3	38	31 934/29.5	12	
YL-6-1	Yangling city, Shaanxi	<i>Populus</i> sp.	Salicaceae	MT166297	108 404	29.7	30	52 378/48.3	38	31 934/29.5	12	
BSHT1	Baishui city, Shaanxi	<i>Juglans regia</i>	Juglandaceae	MT166292	108 388	29.7	30	52 378/48.3	38	30 917/28.5	12	
Lius-YL-4	Yangling city, Shaanxi	<i>Salix babylonica</i>	Salicaceae	MT166293	108 294	29.7	30	52 422/48.4	38	31 780/29.3	12	
SLBM-2-2	Xi'an city, Shaanxi	<i>Punica granatum</i>	Punicaceae	MT166294	105 928	29.6	29	50 120/47.3	36	31 716/29.9	12	
<i>B. kuwatsukai</i> isolates												
PGYT19	Yantai city, Shandong	<i>Malus domestica</i>	Rosaceae	MG593780	124 609	29.7	34	67 714/54.3	40	37 704/30.3	14	
PGLT3	Yangling city, Shaanxi	<i>Malus domestica</i>	Rosaceae	MG593777	120 554	29.4	33	63 663/52.8	38	37 701/31.3	14	
PGZH18	Zhengzhou city, Henan	<i>Malus domestica</i>	Rosaceae	MG593782	119 669	29.2	33	62 770/52.5	38	37 709/31.5	14	
PG2	Yangling city, Shaanxi	<i>Malus domestica</i>	Rosaceae	KY801667	118 034	29.2	32	61 142/51.8	37	37 702/31.9	14	
PGYC4	Yuncheng city, Shanxi	<i>Malus domestica</i>	Rosaceae	MG593779	118 031	29.2	32	61 140/51.8	37	37 701/31.9	14	

^aIntronic and intergenic overall length and percentage in the whole mitogenome are given.

(Torriani *et al.*, 2008). The 17 mitogenomes are complete with no gaps, and each mitogenome was represented in a single circular contig respectively.

Sequence annotation

Gene annotation was performed with MFannot (<http://megasun.bch.umontreal.ca/RNAweasel/>, last accessed date: 04-28-2021) using the NCBI translation Table 4 (The Mold, Protozoan, and Coelenterate Mitochondrial Code and the Mycoplasma/Spiroplasma Code). MFannot annotations were checked by GeSeq (Tillich *et al.*, 2017) and manually checked to confirm gene boundaries as well as intron–exon boundaries by aligning the predicted genes with their orthologues in closely related fungal species. To predict the types of identified HEGs, the coding proteins were searched against the NCBI nr and Pfam databases (<http://pfam.xfam.org>, last accessed date: 04-28-2021). Intron nomenclature was based on the position of the insertion sites of the introns (Johansen and Haugen, 2001; Zhang and Zhang, 2019). The intronic pair was examined by using EMBOSS Stretcher global alignment (<https://www.bioinformatics.nl/cgi-bin/emboss/stretcher>, last accessed date: 05-18-2021), and the duplication events between mitogenome and nucleic genome were examined by BLASTN v. 2.9.0. The graphical map of mitochondrial genome was created using OrganellarGenomeDraw (OGDRAW) v. 1.3.1 tool (Greiner *et al.*, 2019).

Phylogenetic analysis

Phylogenetic analyses were performed by using concatenated amino acid sequences of 12 mitochondrion-encoded proteins. The mitogenomes of selected Dothideomycete species (*Bipolaris sorokiniana*, *Stemphylium lycopersici*, *Parastagonospora nodorum*, *Zymoseptoria tritici*, *Shiraia bambusicola* and *Zasmidium cellare*) were obtained from NCBI (Table S2). The mitogenome of *Zymoseptoria tritici* was used as the outgroup. Best-fit partitioning schemes and models of evolution for each subset were determined according to Prottest v. 3.4.2 (Darriba *et al.*, 2011). Phylogenetic relationships based on the 12 genes were inferred using Bayesian inference (BI) approaches implemented in MrBayes v. 3.2.7 with four steps: (i) prset aamodelpr = fixed (Cprev+G + F); (ii) mcmc; (iii) sump burnin = 500; (iv) sumt burnin = 500 (Ronquist *et al.*, 2012), and maximum likelihood (ML) trees were constructed in RAxML with ‘-f a -x 12345 -p 12345 -# 100 -m PROTGAMMACPREVX’ (Stamatakis, 2006).

Comparison of mitogenomes of *Botryosphaeria* species

The mitogenomic sequences of *Botryosphaeria* isolates were aligned using the online program MAFFT v. 7

(<http://mafft.cbrc.jp/alignment/server/>, last accessed date: 04-28-2021) (Kato and Standley, 2013). For genes with intron presence/absence variations among the isolates studied, exonic sequences between intron-carrying and intron-lacking isolates were compared to see if there were characteristic exonic sequences that flanked introns. The nucleotide variations of intronic and exonic sequences were summarized using DnaSP v. 6.12.03 (Rozas *et al.*, 2017). A comparative map was generated under default alignment parameters in Mauve v. 2.4.0 (Darling *et al.*, 2010) to visualize variations in the genomic architecture. An UPGMA dendrogram based on intron presence/absence patterns at every intron locus assessed from all isolates was constructed based on Jaccard similarity using the online program DendroUPGMA (<http://genomes.urv.cat/UPGMA/>, last accessed date: 04-28-2021). Presumed gain/loss history for each intron identified in isolates of *B. dothidea* and *B. kuwatsukai* was traced using the parsimony method in Mesquite v. 3.51 (<http://mesquiteproject.org>, last accessed date: 04-28-2021), and the above phylogeny constructed using nucleotide data was used in this analysis. For both DendroUPGMA and Mesquite analyses, intron absence/presence patterns were coded as 0/1 matrices. To infer the ancestral intron distribution pattern, we performed a Bayesian binary MCMC analysis under the CpREV + G model based on the obtained BI tree (similar to the BI settings above) in RASP v. 4.0 (Yu *et al.*, 2015). The *t*-test was calculated by R script with ‘geom_signif (comparisons = list(c(“sample1”, “sample2”), test = “t.test”))’ (<https://rdocumentation.org/packages/ggsignif/versions/0.6.1>, last accessed date: 05-18-2021).

F_{ST} and Ka/Ks analysis

F_{ST} was calculated using vcftools v. 0.1.14 with ‘--vcf merge.vcf --weir-fst-pop *B.dothidea*_population_1.txt --weir-fst-pop *B.kuwatsukai*_population_2.txt --out result_Fst’ (Danecek *et al.*, 2011). The merge.vcf was obtained using ‘samtools + bcftools’ pipeline (Danecek *et al.*, 2021). The ratio of nonsynonymous (Ka) to synonymous (Ks) nucleotide substitution rates (Ka/Ks) was calculated by ParaAT v. 2.0 and Ka/Ks _Calculator v. 2.0 with YN model (Wang *et al.*, 2010; Zhang *et al.*, 2012).

Results

Isolate selection and identification

In previous research, we reappraised the host range of *B. dothidea* and *B. kuwatsukai*, and found that the host range of *B. kuwatsukai* is apparently narrower, whereas *B. dothidea* is able to infect a wide range of hosts (Xu *et al.*, 2015). To understand the diversity of two

species on apple, we chose five *B. dothidea* isolates (PG45, PGLWX, PGLB9, PGZH16 and PGZH20) and five *B. kuwatsukai* isolates (PGYT19, PGLT3, PGZH18, PG2 and PGYC4) from apple. With the wide host range of *B. dothidea* in mind, seven isolates from other hosts were chosen for comparative analysis (Table 1).

The *Botryosphaeria* isolates were collected from different provinces including Shaanxi, Hennan, Shandong and Shanxi, with their host species from different families, including Rosaceae, Vitaceae, Ebenaceae, Salicaceae, Juglandaceae, Salicaceae and Punicaceae (Table 1). Based on molecular phylogenetic analysis of the combined nuclear DNA locus data of ITS and EF-1 α (Table S1), we identified 17 isolates in two species, *Botryosphaeria dothidea* and *B. kuwatsukai* (Fig. S1; Table 1).

Botryosphaeria kuwatsukai mitogenome sizes were significantly larger than those of *B. dothidea*

We compared these 17 mitogenomes with regard to sizes, gene contents and arrangement, and intron characteristics. Sizes of the 12 *B. dothidea* mitogenomes ranged between 105 700 and 114 832 bp with G + C content from 29.4% to 29.7%, whereas the five *B. kuwatsukai* mitogenomes ranged in size from 118 031 to 124 609 bp with G + C content from 29.2% to 29.7% (Table 1). The mitogenome sizes of the *B. kuwatsukai* group were significantly larger than that for the *B. dothidea* group ($P < 0.05$) (Fig. S2). For *B. dothidea*, intronic regions accounted for 47.1%–49.2% of the whole mitogenome, whereas for *B. kuwatsukai*, intronic regions accounted for more than half of the whole mitogenome (51.8%–54.3%). All 17 sequenced mitogenomes

contained 13 core genes involved in four cytochrome *c* oxidase subunits (*cox1*, *cox2*, *cox3* and *cob*), two *atp* synthase subunits (*atp6* and *atp9*) and seven NADH dehydrogenase subunits (*nad1*, *nad2*, *nad3*, *nad4*, *nad4L*, *nad5* and *nad6*), but *atp8* was missing. The fungi *Stemphylium lycopersici*, *Parastagonospora nodorum* and *Shiraia bambusicola* have also lost the *atp8* and *atp9* genes, and all fungi examined contained the 12 core genes (Table S2). The untranslated genes of the small and large ribosomal RNA (rRNA) subunits (*rns* and *rnl* respectively) and a set of transfer RNA (tRNA) genes were all present on the forward strand (Fig. 1A and B). The ribosomal protein S3 (*rps3*) was also detected in all 17 isolates. The number of tRNA genes ($n = 28$), tRNA total length (2087 bp) and tRNA cluster were assessed for the 17 isolates. The 28 tRNA genes coded for all 20 standard amino acids. All 13 core protein-coding genes started with the canonical AUG initiation codon except *cox1* with UUG and *cox2* with GUG. The preferred stop codon was UAA, with the exception of *cox2*, *atp6*, *nad1* and *atp9*, which used UAG, and *cox1* with UGA.

Botryosphaeria dothidea and *B. kuwatsukai* (*Botryosphaeriales*) were found to have among the largest mitogenome sizes (106 kb–125 kb) compared to published fungal species in Dothideomycetes, including 138 kb for *Bipolaris sorokiniana* (Pleosporales), 76 kb for *Stemphylium lycopersici* (Pleosporales), 50 kb for *Parastagonospora nodorum* (Pleosporales), 44 kb for *Zymoseptoria tritici* (Capnodiales), 39 kb for *Shiraia bambusicola* (Pleosporales) and 24 kb for *Zasmidium cellare* (Capnodiales) (Table S2). The intron numbers of *B. dothidea* and *B. kuwatsukai* ($n = 29$ –34) were

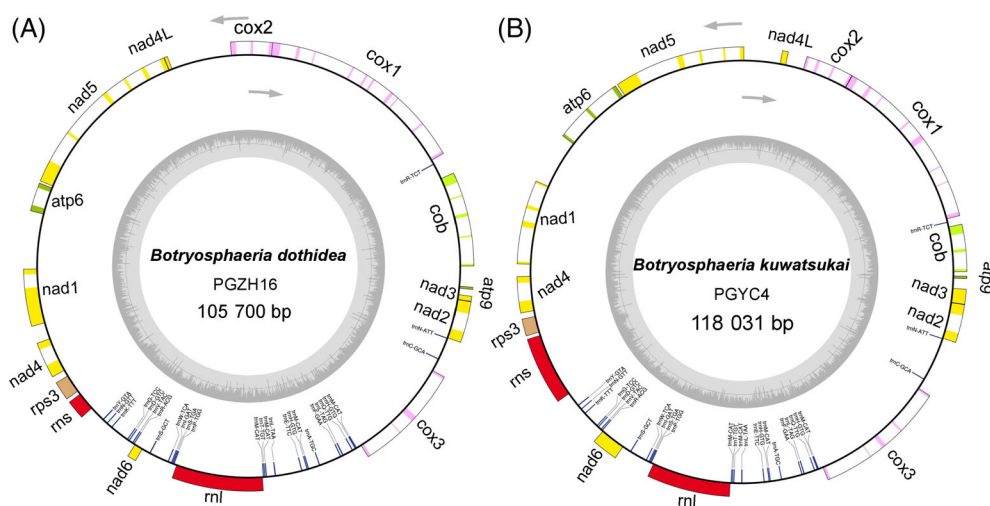


Fig. 1. Circular complete graphic mitogenome maps of *B. dothidea* PGZH16 (A) and *B. kuwatsukai* PGYC4 (B). The circular map created by OGDRAW contained two ribosomal RNA genes, 13 standard protein-coding genes of the oxidative phosphorylation system, 28 tRNA genes. All tRNA were actually located outside the circle, for beauty, they were placed inside the circle manually. Arrows indicate transcription directions. The inner grey rings show the G + C content of these genomes. [Color figure can be viewed at wileyonlinelibrary.com]

significantly expanded ($P < 0.05$) (Table S2). The gene order in these examined Dothideomycetes was similar within genus but was not consistent in different genera (Table S2).

A variety of intronic patterns within *B. dothidea*

All mitogenomes contained *rnl*, *rns*, tRNA genes and standard genes coding proteins; however, the genomes varied in size ranging from 105.7 to 114.8 kb. Isolates having larger mitogenome sizes contained higher intron numbers (Table 1). By mitogenomic alignment analysis, intron presence/absence dynamics were detected among 12 *B. dothidea* isolates (Fig. 2A). For instance, the 2521–2648 bp Bdo.cobS100 sequences were present in most isolates but absent in PGZH20 and PGZH16 both from apple, which likely contributed to their smaller sizes. Although Bdo.cobS100 was present in SLBM-2-2 from pomegranate, the 2380–2447 bp Bdo.nad5P9350 sequence was absent, which also contributed to its smaller size. The 1625–1626 bp Bdo.cox1P15445 sequences were present only in TCPTT1 from grape and PG45 from apple, which made their mitogenome sizes relatively large. In addition to intron

presence/absence in mitochondrial genes, 2421-bp and 1769-bp insertions were found in the *cob*-trnR and *rns*-trnY intergenic regions of TCPTT1 respectively, contributing to the largest size among mitogenomes in this study.

These mitochondrial genome size variations can largely be explained by the presence/absence of introns in certain genes and additional length variations among intergenic regions. Specifically, 28 introns were found in all 12 *B. dothidea* mitogenomes: four *cob*, nine *cox1*, two *cox2*, four *nad5*, one *atp6*, one *nad1*, one *nad4*, three *cox3*, one *nad2* and two *rnl* genes. Around 80% of predicted introns belonged to the group I intron family with several specific types: IA, IB, IC₂, ID and I derived (Fig. 3B). Only two group II intron types were detected in Bdo.cobS100 and Bdo.cox1S202. About 90% of *B. dothidea* intronic ORFs were classified with the ‘LAGLIDADG’ type endonuclease. Introns of Bdo.cox1P9480, Bdo.cox3P220 and Bdo.cox3P4669 contained two connected intronic ORFs. Interestingly, the two connected intronic ORFs in Bdo.cox1P9480 encoded one ‘LAGLIDADG’ type endonuclease, and another one was a ‘GIY-YIG’ type endonuclease. Strains PGZH20 and PGZH16 contained no Bdo.cobS100 group II intron, and SLBM-2-2 lost the Bdo.

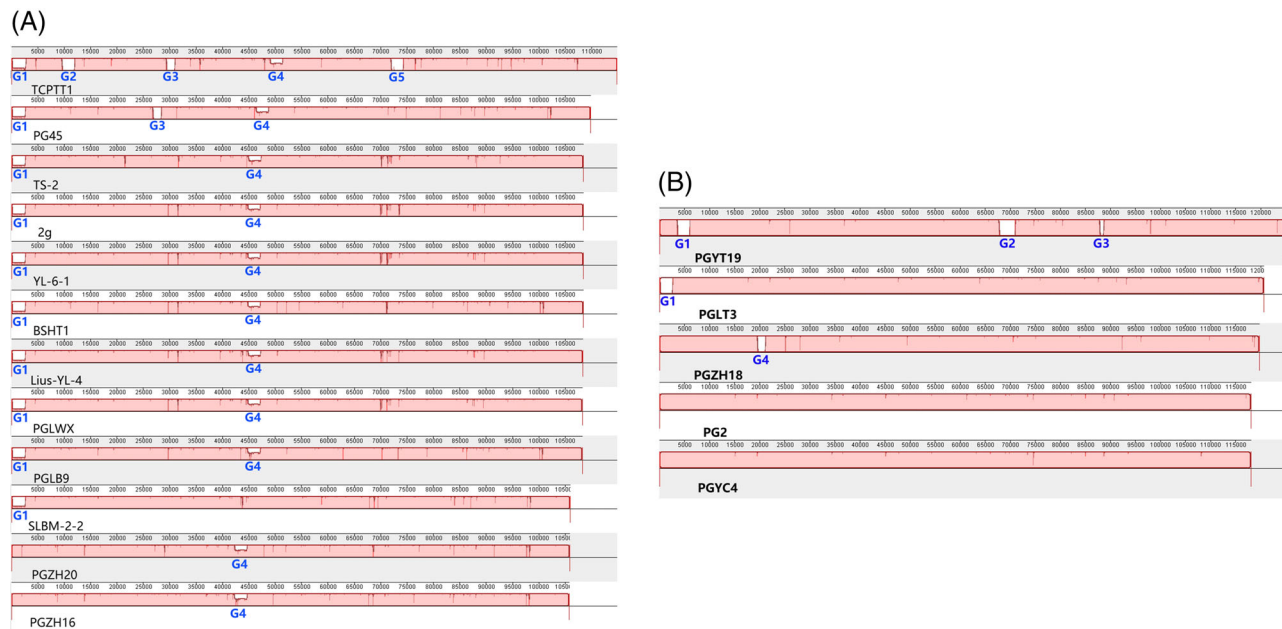


Fig. 2. Alignment of 12 *B. dothidea* mitogenomes and five *B. kuwatsukai* mitogenomes.

A. Numbered scale bars indicate distance in base pairs, and vertical bars indicate sequence similarity. Size differences among the 12 mitogenomes were mainly due to presence/absence of introns in certain genes (G1, G3 and G4). Two DNA insertions of intergenic region (G2 and G5) made TCPTT1 the longest size of all *B. dothidea* mitogenomes. G1, the 2521–2648 bp Bdo.cobS100 sequences present in all strains but absent in PGZH20 and PGZH16; G2, the 2421 bp insertion located at the *cob*-trnR intergenic region present only in TCPTT1; G3, the 1625–1626 bp Bdo.cox1P15445 sequences present only in TCPTT1 and PG45. G4, the 2380–2447 Bdo.nad5P9350 sequences absent only in SLBM-2-2; G5, the 1769 bp insertion located at the *rns*-trnY intergenic region present only in TCPTT1.

B. Numbered scale bars indicate distance in base pairs, and vertical bars indicate sequence similarity. Size differences among the five mitogenomes were mainly due to presence/absence of introns in certain genes (G1, G2 and G4). G1, the 1522 bp Bku.cobP202 sequences present only in PGYT19 and PGLT3 and showed rearrangement between these two strains. G2, the 3250 bp Bku.ms3720 sequences present only in PGYT19. G3, the 852 bp DNA fragment inserted in Bku.mL87138 sequences of PGYT19. G4, the 1625 bp Bku.cox1P14777 sequences present only in PGZH18. [Color figure can be viewed at wileyonlinelibrary.com]

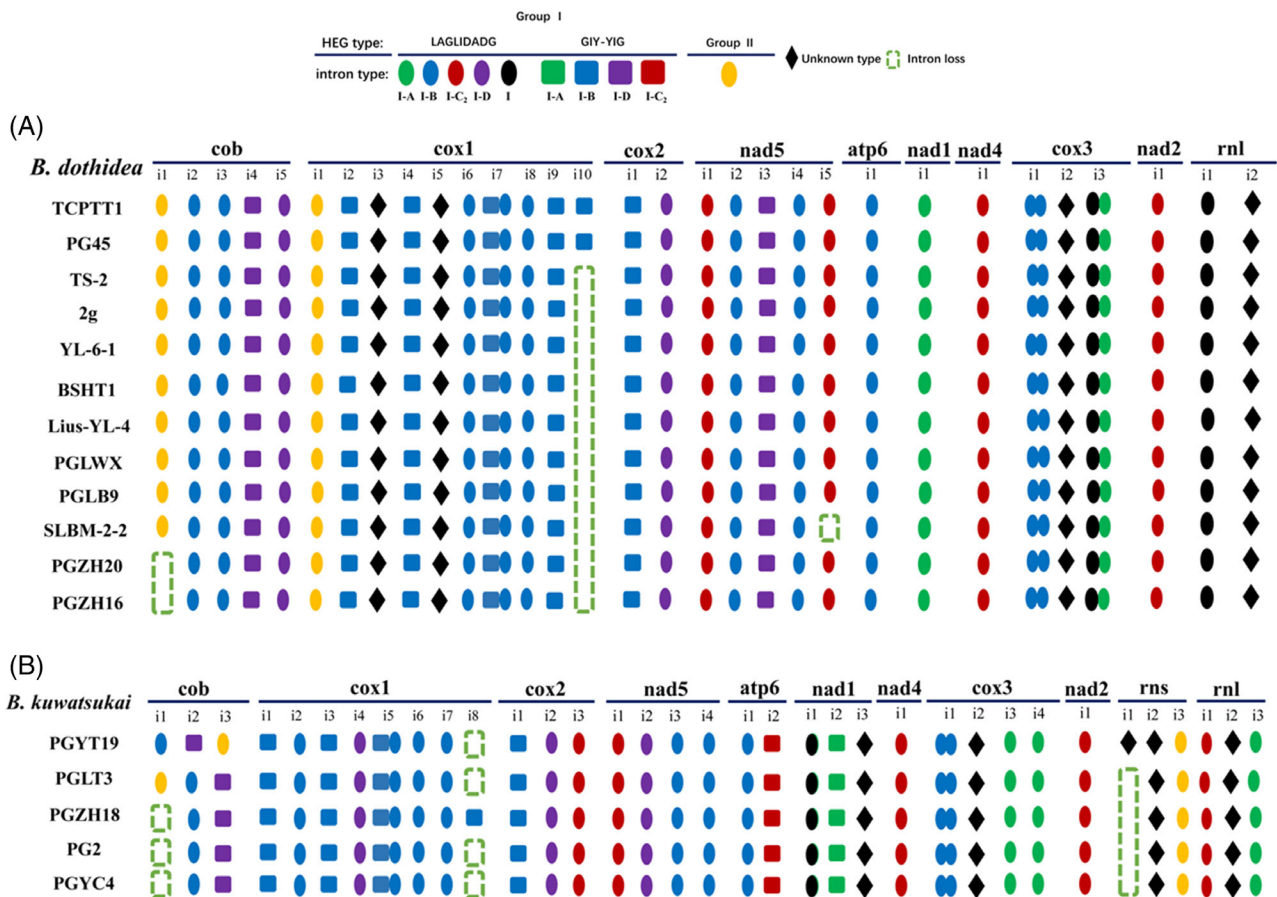


Fig. 3. The *B. dothidea* and *B. kuwatsukai* mitogenome introns.

A. The introns classified into groups I-A, I-B, I-C2 and I-D and harbour homing endonuclease genes (HEG) were classified into 'LAGLIDADG' and 'GIY-YIG' types. The distribution patterns of 29–31 introns were shown.

B. The introns classified into groups I-A, I-B, I-C2 and I-D and harbour homing endonuclease genes (HEG) were classified into 'LAGLIDADG' and 'GIY-YIG' types. The distribution patterns of 32–34 introns were shown. [Color figure can be viewed at wileyonlinelibrary.com]

nad5P9350 IC₂ intron and its intronic 'LAGLIDADG' endonuclease (Fig. 3B). In contrast, strains PG45 and TCPTT1 gained a Bdo.cox1P15445 IB intron with a 'GIY-YIG' type endonuclease (Fig. 3B).

We compared genetic diversity of intron sequences with their host gene exon sequences. Overall, exons generally showed a higher variation frequency than introns (6.55 vs. 6.05). Nucleotide variations were observed in exonic sequences of *cob*, *cox1*, *nad1*, *nad3*, *nad4*, *nad5*, *rps3* and rRNA genes. For protein-coding genes, the highest variation frequency was 5.56%, occurring in *cob* exons with one 'TTTATAAAAATA' indel event and 64 SNPs, resulting in 16 amino acid changes. Other exonic variations were all non-synonymous changes but for no amino acid changes observed in *nad5*. Indels were more frequently found in introns compared to exons (4 vs. 36) (Table S3).

Comparison between isolates carrying introns and isolates lacking introns identified characteristic nucleotides at upstream/downstream exon sequences (Table S4). A co-

conversion between Bdo.nad5P9350 and upstream exon was observed, such as 'ATGACGGGATTCTATTC' existing in isolates without intron, but 'ATGACCGGTTTTTATTC' existing in isolates with introns (Table S4). This change did not affect the protein sequence of the *nad5* gene.

A variety of intronic patterns within B. kuwatsukai

Five *B. kuwatsukai* isolates from apple were chosen for analysis of intra-species mitogenomic diversity (Table 1). By whole mitogenomic alignment analysis, intron presence/absence dynamics were detected among five *B. kuwatsukai* isolates (Fig. 2B). For instance, the 1522 bp Bku.cobP202 sequence was present only in PGYT19 and PGLT3, but, the Bku.cobP202 fragment was rearranged between two isolates. The 3250 bp Bku.mS70919 sequence and the 852 bp Bku.mL87138 insertion were present only in PGYT19, making it the largest among *B. kuwatsukai* isolates examined. The 1625 bp Bku.cox1P14777 sequence was present only in

PGZH18. *Botryosphaeria kuwatsukai* mitogenomes together contained 32 different introns: two *cob*, seven *cox1*, three *cox2*, four *nad5*, two *atp6*, three *nad1*, one *nad4*, four *cox3*, one *nad2*, two *rns* and three *rnl* genes (Fig. 3B). About 78% of the predicted introns belonged to the group I intron family which could be divided into several specific types: IA, IB, IC₂, ID and I derived (Fig. 3B). Only two group II introns were detected, and these were located in Bku.cobP202/Bku.cobP3566 and Bku.mS73334. About 69% of the *B. kuwatsukai* intronic ORFs belonged to 'LAGLIDADG' type endonuclease. Introns of Bku.cox1P9067 and Bku.cox3P220 contained two continuous intronic ORFs (Fig. 3B). Interestingly, the two continuous intronic ORFs in Bku.cox1P9067 encoded one 'LAGLIDADG' type endonuclease and one 'GIY-YIG' type endonuclease. Strains PGZH18, PG2 and PGZH16 contained no Bku.cobP202 introns, but PGZH18 gained a Bku.cox1P14777 intron. Strain PGYT19 gained a Bku.mS3720 unclassified type intron (Fig. 3B).

We compared genetic diversity of intron sequences with their host gene exon sequences. Unlike *B. dothidea*, introns of *B. kuwatsukai* generally showed a higher variation frequency than exons (1.08% vs. 0.29%) (Table S5). Nucleotide variations were observed only in exonic sequences of *cox1* with five SNP mutations. These variations were synonymous changes. Indels were more frequently found in introns compared to exons (10 vs. 5). Comparison between isolates carrying introns and isolates lacking introns identified characteristic nucleotides at upstream/downstream exon sequences (Table S4). A co-conversion between Bku.cox1P14777 and upstream/downstream exon was observed, such as 'TTGGTGTTAATCTTACTTTCTTCCCT' from upstream of the inserted intron existing in isolates without the intron, but 'TAGGGGTTAATCTTACTTTCTTCCCT' was found in isolates with the intron; and 'GTTTACAA GGAATGCCGA' from downstream of the intron was found in isolates without the intron, but 'GTCTACAAGGAAT GCCTA' was found in isolates with intron (Table S4). The five SNP changes of the *cox1* gene were synonymous mutations. The Ka/Ks ratios in 12 *B. dothidea* isolates and 5 *B. kuwatsukai* isolates were all unavailable, and between *B. dothidea* and *B. kuwatsukai* were very low, ranging from 0.0 to 0.87 (Fig. S3), suggesting that all protein-coding genes were under negative (purifying) selection.

Intron variations probably contribute to speciation and interspecific genetic diversity of B. dothidea and B. kuwatsukai

We chose five *B. dothidea* isolates with different intronic patterns according to Fig. 2A, and four *B. kuwatsukai* isolates with different patterns according to Fig. 2B, to analyse the interspecific genetic diversity. Mitogenome-wide

comparison between *B. dothidea* and *B. kuwatsukai* species indicated 11 homologous blocks (HB) shared between the two species (Fig. 4). We found five HBs (HB2: 247 bp, HB3: 290 bp, HB5: 255 bp, HB7: 299 bp and HB8: 858 bp) rearranged between two species (Fig. 4). The mobile elements in HB2 and HB3 all belonged to group IB intronic sequences, and those in HB5, HB7 and HB8 belonged to group IC₂. The length of HB1 in *B. dothidea* isolates was significantly larger than that of *B. kuwatsukai*, mainly due to 4–6 *cob* and *cox1* intronic presence/absence events. In contrast, the HB9, HB10 and HB11 sizes of *B. kuwatsukai* were significantly larger than that of *B. dothidea*, mainly due to *nad1* of *B. kuwatsukai* gained two more introns than *B. dothidea*; *rns* gained 2–3 intronic insertions than *B. dothidea*; *rnl* gained a large insertion compared to *B. dothidea*; *B. kuwatsukai* gained trnC-trnN intergenic region insertions.

The possible origins of mitochondrial introns in *B. dothidea* and *B. kuwatsukai* were examined. First, the possibility of intra-mitogenomic duplication was tested by performing BLASTN analyses of these introns against each other in *B. dothidea*. We found significant sequence similarities only between Bdo.nad5P3441 and Bdo.nad5P5355 intron pairs at 88.5% identity with 182 bp alignment length (Table S6). This intronic pair was examined by using EMBOSS Stretcher global alignment, and only 31.7% identity was obtained. The same analysis was applied in *B. kuwatsukai* mitogenomes, and for maximum global alignment identity, low similarity was observed in the intronic pair (Table S7). Based on comparisons with published nuclear genomes which includes *B. dothidea* (GCA_004016265.1) and *B. kuwatsukai* (GCA_004016305.1) (Wang et al., 2018a), we did not detect obvious duplication events between mitogenomes and nuclear genomes by BLASTN.

There was evidence of horizontal transfer for two *Botryosphaeria* introns when BLASTN searches against the public nucleotide database were performed (Tables S8 and S9). Most introns, 57% in *B. dothidea* and 49% in *B. kuwatsukai*, showed high sequence identities to orthologous introns found in non-Dothideomycetes including Leotiomyces, Eurotiomyces and Sordariomyces fungi (Tables S8 and S9). Interestingly, the Bdo.cobP8060 intronic sequence of *B. dothidea* might have been horizontally transferred from *Moniliophthora roreri* in Basidiomycota, with 99% query coverage and 83% identity (Table S8).

The *B. dothidea* and *B. kuwatsukai* mitogenomes contained seven different intron distribution patterns (Table S10), and none of these was shared between the two species (Fig. 5A). In *B. dothidea*, strain SLBM-2-2 displayed an exclusive pattern A with a Bdo.nad5P9350 intronic absence. Intron distribution pattern B was found in PG45 and TCPTT1, which were the only mitogenomes

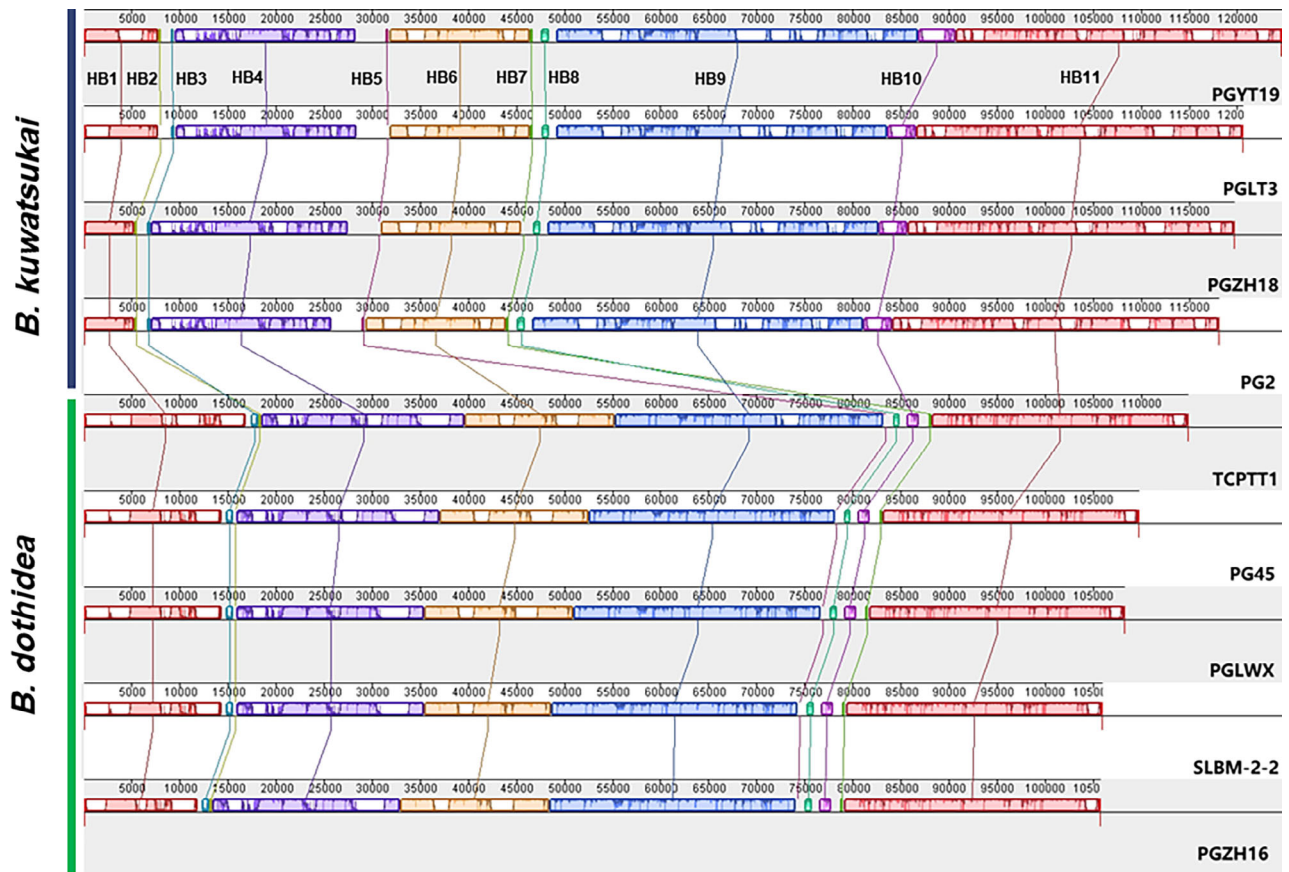


Fig. 4. Genome-wide comparison between *B. dothidea* and *B. kuwatsukai*. It shows the homologous blocks shared among the mitogenomes based on the Mauve analysis, and it also showed the five homologous block (HB2: 247 bp alignment length, HB3: 290 bp alignment length, HB5: 255 bp alignment length, HB7: 299 bp alignment length, and HB8: 858 bp alignment length) rearrangement between two species. Gaps show unique sequences for each mitogenome. [Color figure can be viewed at wileyonlinelibrary.com]

with Bdo.cox1P15445. Pattern C included seven isolates without Bdo.cox1P15445. PGZH20 and PGZH16 formed pattern D, due to their Bdo.cobS100 loss. In *B. kuwatsukai*, intron patterns E, F and G were found (Fig. 5A). PGYT19 and PGLT3 lost the Bku.cox1P14777 intron, forming pattern E. The Bku.cobP202 intron absence and Bku.cox1P14777 present made PGZH18 an exclusive pattern F. Absence of introns Bku.cobP202 and Bku.cox1P14777 made up pattern G in PGYC4 and PG2.

We constructed an ML phylogenetic tree using concatenated protein sequences of 12 standard mitochondrial protein-coding genes (*cob*, *cox1*, *cox2*, *nad4L*, *nad5*, *atp6*, *nad1*, *nad4*, *nad6*, *cox3*, *nad2* and *nad3*) from 17 isolates of *Botryosphaeria* and other isolates from Pleosporales and Capnodiales (Fig. S4). The *B. kuwatsukai* isolates clustered together with 100% bootstrap support, and the *B. dothidea* isolates clustered together with 74% bootstrap support, and these two species were distinguished by mitogenomic phylogeny with 100% bootstrap support (Fig. S4). In addition, mean F_{ST}

value between *B. dothidea* and *B. kuwatsukai* was 0.298, indicating these two populations were strong genetic differentiation.

Based on inferences from ancestral intron distribution patterns, the tree from RASP roots nodes of *B. dothidea* and *B. kuwatsukai* was suggested to have the intron presence/absence patterns C and G respectively (Fig. 5B). Intron gain/loss event investigations showed that Bku.atp6P3205 and Bku.cobP3566 were each lost once in *B. dothidea* and *B. kuwatsukai*, whereas Bku.nad5P5695 and Bku.cobP202 might have experienced two and three loss events respectively. Bdo.cox1P15445 might have experienced two independent gain events occurring in the two species (Fig. 6).

Discussion

To date, many mitogenomes have been published for members of the Dothideomycetes, such as the phytopathogenic fungus *Bipolaris sorokiniana* (Pleosporales) (Song *et al.*, 2020), wheat pathogens *Parastagonospora*

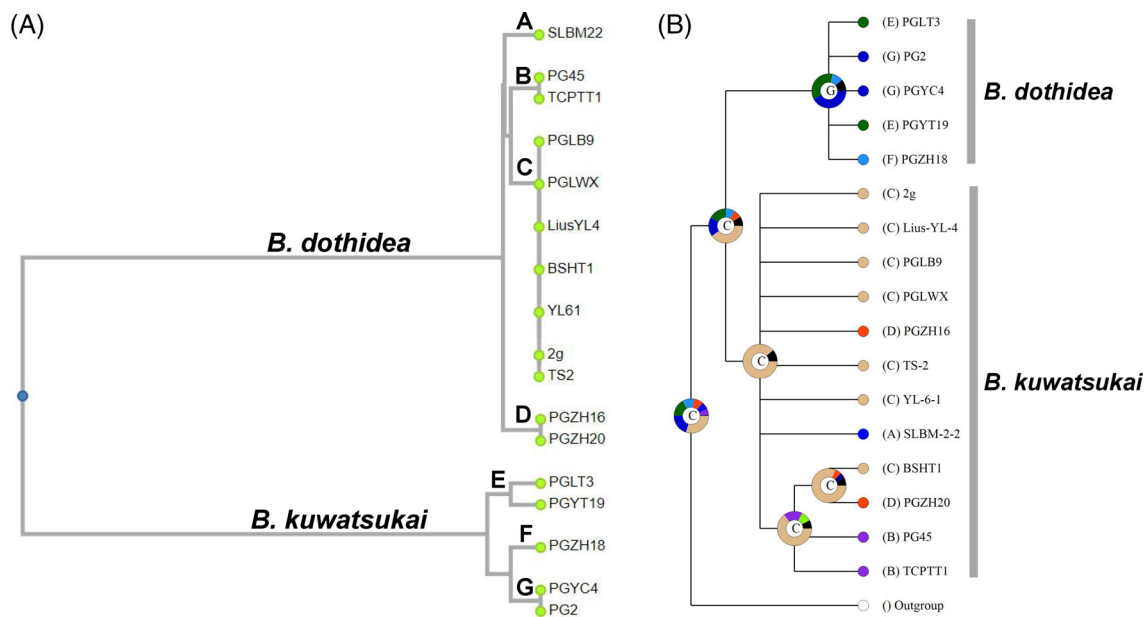


Fig. 5. Ancestral intron distribution pattern analysis of *B. dothidea* and *B. kuwatsukai*.

A. Dendrograms constructed based on intron presence/absence patterns (Please also refer to Supporting Information Table S10 for details).

B. Pattern analysis by Bayesian binary MCMC analysis in RASP software. Nodes are displayed most likely states only. Pie charts at each node represent the marginal probabilities for each alternative intron distribution pattern (denoted with the respective letters A–G showing in Fig. 5A). Partially black coloured pie charts indicate that none of the defined patterns was obtained. *Parastagonospora nodorum* was used as an outgroup. [Color figure can be viewed at wileyonlinelibrary.com]

nodorum (Pleosporales) (McDonald *et al.*, 2019), *Zymoseptoria tritici* (Capnodiales) (Torriani *et al.*, 2008), *Shiraia bambusicola* (Pleosporales) (Shen *et al.*, 2015), *Zasmidium cellare* (Capnodiales) (Goodwin *et al.*, 2016) and *Stemphylium lycopersici* (Pleosporales) (Franco *et al.*, 2017). All of these species have mitogenomes of small to moderate sizes, ranging from 24 to 76 kb, except for *Bipolaris sorokiniana* at 138 kb. This is the first report of the mitochondrial genomes of *B. dothidea* and *B. kuwatsukai* (Botryosphaerales). Among sequenced Dothideomycetes, these were large mitogenome sizes (106–125 kb) due to significant expansions of introns and ORFs insertions. These expanded introns were possibly obtained by horizontal gene transfer from non-Dothideomycetes fungal species, which is a phenomenon common in the fungal kingdom (Wang *et al.*, 2018b; Fan *et al.*, 2019).

We performed intraspecific comparative analysis of *B. dothidea* mitogenomes using 12 isolates from geographically distant hosts, and of *B. kuwatsukai* using five isolates from geographically distant apples. We found that intraspecific comparisons showed intron polymorphisms in terms of presence or absence. In *B. dothidea*, up to 31 introns were present in each of the isolates, and there were 29 common to all 12 isolates, while three introns were only found in certain isolates. The number of *B. kuwatsukai* introns (32–34) was larger than that of *B. dothidea*, with 13 shared between all isolates. There were

three intronic loci in certain isolates only, such as Bku. cox1P14777 only in PGZH18. The phenomenon of mitochondrial intron presence/absence dynamics at the intra-specific level has been previously reported for non-Dothideomycetes fungi, such as *Podospira anserina* (Cummings *et al.*, 1990), *Rhizophagus irregularis* (Formey *et al.*, 2012), *Hirsutella thompsonii* (Wang *et al.*, 2018b), *Isaria cicadae* (Fan *et al.*, 2019) and several yeasts (Jung *et al.*, 2012; Freel *et al.*, 2014; Xiao *et al.*, 2017). Based on inferences from ancestral intron distribution patterns, *B. dothidea* and *B. kuwatsukai* dynamic introns might have experienced two to three gain or loss events. We suggest that *B. kuwatsukai* intronic gains or losses might have occurred after the fungus split from its putative sister species, *B. dothidea* (intron pattern C to D). Dynamic introns of non-Dothideomycetes fungi *Hirsutella thompsonii* and *Isaria cicadae* were reportedly gain or loss events (Wang *et al.*, 2018b; Fan *et al.*, 2019), indicating that intron dynamic evolution might be a common phenomenon in Fungi.

Apple ring rot inflicts severe economic losses in the main apple-producing areas of China and Japan (Ogata *et al.*, 2000; Tang *et al.*, 2012). In Japan, the causal organisms were identified as *Botryosphaeria dothidea* and *B. berengeriana* f. sp. *piricola* (syn. *Physalospora piricola*) (Koganezawa and Sakuma, 1984). In the United States, a similar disease, white rot of apple has been reported, and *B. dothidea* was described as the causal

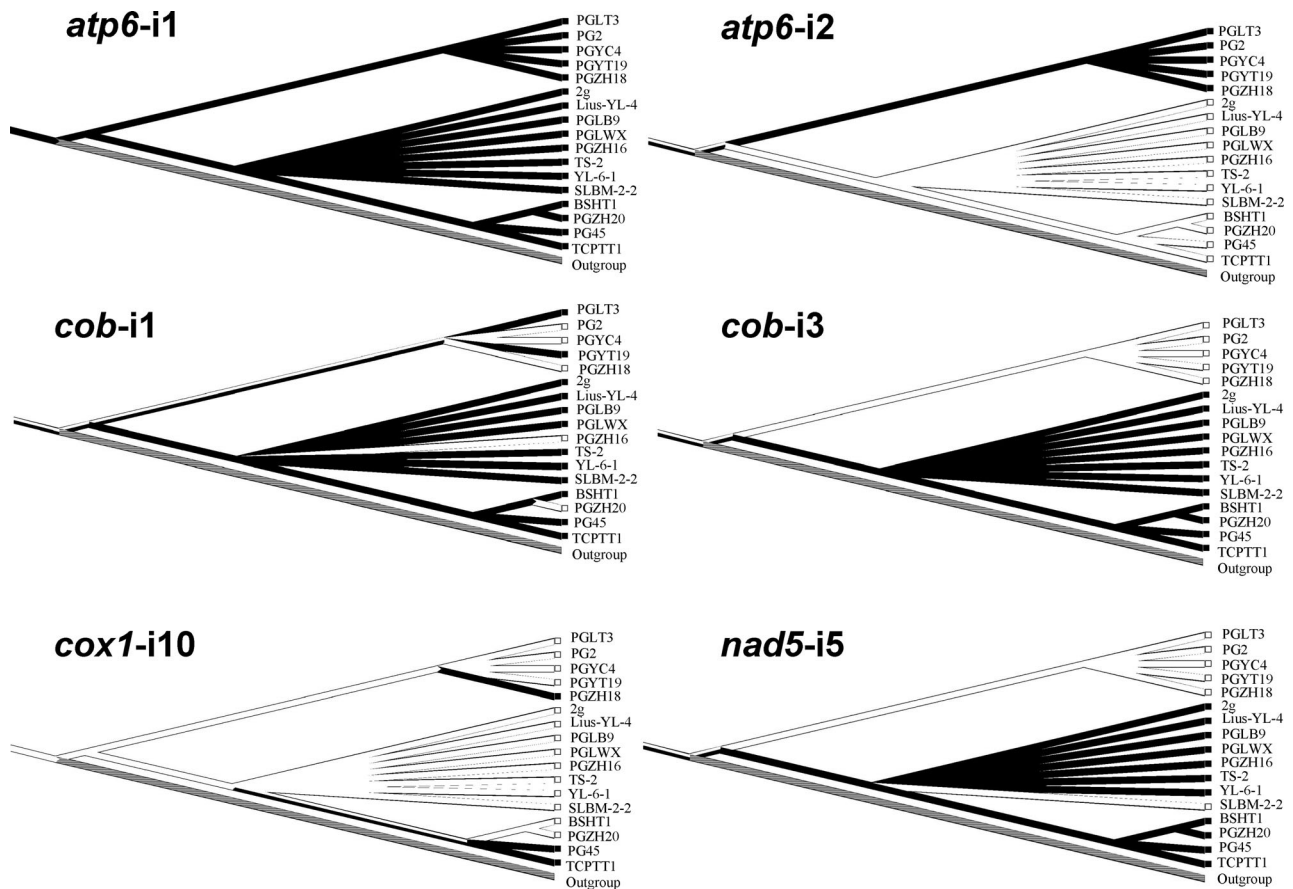


Fig. 6. Inference of gain/loss events of introns identified in *B. dothidea* and *B. kuwatsukai*. The six different intron distribution patterns were shown, each pattern was represented by one intron. Hollow white lines indicate the absence of an intron in a given strain, and solid black lines indicate the presence of an intron in corresponding strain.

agent. Our previous study reappraised the aetiology of apple ring rot using polyphasic taxonomy, and considered *B. kuwatsukai* (syn. *B. berengeriana* f. sp. *piricola*) and *B. dothidea* to be separate species (Xu *et al.*, 2015). The results also showed that apple ring rot in eastern Asia might be the same disease as white rot in the United States (Xu *et al.*, 2015), and our genomic analysis of these two species supported this contention (Wang *et al.*, 2018a). In this study, these two species were distinguished further by the phylogeny of mitogenomes.

Previous research showed that there was a marked difference between the two species groups by RAPD and ISSR analysis (Huang and Liu, 2001; Peng *et al.*, 2011). In this study, *B. dothidea* and *B. kuwatsukai* displayed seven intronic distribution patterns, unique to each species. The intronic distribution patterns of the mitogenomes could be used as a marker for *Botryosphaeria* population structure analysis and dynamics in ecology. It will be beneficial to the ecological control of diseases causing by *Botryosphaeria* species. Further investigation should be carried out with more isolates to

reveal whether there are more intronic types among isolates of these two species and whether these different patterns correlate with host and geography.

Intraspecific genetic diversity of mitogenomes of *B. dothidea* was significantly higher than that of *B. kuwatsukai* based on genetic diversity analysis. Almost all exonic variations in *B. dothidea* mitogenomes were nonsynonymous changes, but only synonymous mutations were found in *B. kuwatsukai*. We speculate that the nonsynonymous changes in the mitogenomes of *B. dothidea* allowed for adaptation to a wider host range and ecological niche, whereas the synonymous mutations with no acid amino changes in mitogenomes of *B. kuwatsukai* resulted from its host specialization (Xu *et al.*, 2015).

Conclusion

In this study, we sequenced the mitochondrial genomes of 17 *B. dothidea* and *B. kuwatsukai* isolates and examined the mitogenomic variation at the population level.

Both species had the largest mitogenome sizes among Dothideomycetes studied, attributable to significant intron expansion, and the expansion may have been through horizontal gene transfer from non-Dothideomycetes fungi. The variation in mitogenomic sizes within and between the two species was mainly caused by the gain or loss of introns. The intronic distribution patterns of the mitogenomes could be useful markers for population diversity. The mitochondrial gene phylogeny supported the separation of *B. dothidea* and *B. kuwatsukai* as independent species, which is consistent with our previous results on genomic analysis and multiple nuclear DNA locus phylogeny.

Acknowledgements

This work was supported by the National Natural Science Foundation of China (31371887), China Agriculture Research System of MOF and MARA (CARS-27) and China Postdoctoral Science Foundation (2020M673420).

References

- Ballard, J.W., and Whitlock, M.C. (2004) The incomplete natural history of mitochondria. *Mol Ecol* **13**: 729–744.
- Bankevich, A., Nurk, S., Antipov, D., Gurevich, A.A., Dvorkin, M., Kulikov, A.S., et al. (2012) SPAdes: a new genome assembly algorithm and its applications to single-cell sequencing. *J Comput Biol* **19**: 455–477.
- Bullerwell, C.E., and Lang, B.F. (2005) Fungal evolution: the case of the vanishing mitochondrion. *Curr Opin Microbiol* **8**: 362–369.
- Burt, A., and Koufopanou, V. (2004) Homing endonuclease genes: the rise and fall and rise again of a selfish element. *Curr Opin Genet Dev* **14**: 609–615.
- Chen, C. (1999) Advances in the research of apple ring rot. *Acta Phytopathol Sin* **29**: 1–7 [in Chinese].
- Chen, S., Zhou, Y., Chen, Y., and Gu, J. (2018) Fastp: an ultra-fast all-in-one FASTQ preprocessor. *Bioinformatics* **34**: i884–i890.
- Cummings, D.J., McNally, K.L., Domenico, J.M., and Matsuura, E.T. (1990) The complete DNA sequence of the mitochondrial genome of *Podospora anserina*. *Curr Genet* **17**: 375–402.
- Danecek, P., Auton, A., Abecasis, G., Albers, C.A., Banks, E., DePristo, M.A., et al. (2011) The variant call format and VCFtools. *Bioinformatics* **27**: 2156–2158.
- Danecek, P., Bonfield, J.K., Liddle, J., Marshall, J., Ohan, V., Pollard, M.O., et al. (2021) Twelve years of SAMtools and BCFtools. *GigaScience* **10**: giab008.
- Darling, A.E., Mau, B., and Perna, N.T. (2010) progressiveMauve: multiple genome alignment with gene gain, loss and rearrangement. *PLoS One* **5**: e11147.
- Darriba, D., Taboada, G.L., Doallo, R., and Posada, D. (2011) ProtTest 3: fast selection of best-fit models of protein evolution. *Bioinformatics* **27**: 1164–1165.
- De Chiara, M., Friedrich, A., Barré, B., Breitenbach, M., Schacherer, J., and Liti, G. (2020) Discordant evolution of mitochondrial and nuclear yeast genomes at population level. *BMC Biol* **18**: 49.
- Egdel, D.R. (2009) Selfish DNA: homing endonucleases find a home. *Curr Biol* **19**: R115–R117.
- Fan, W.W., Zhang, S., and Zhang, Y.J. (2019) The complete mitochondrial genome of the Chan-hua fungus *Isaria cicadae*: a tale of intron evolution in Cordycipitaceae. *Environ Microbiol* **21**: 864–879.
- Formey, D., Molès, M., Haouy, A., Savelli, B., Bouchez, O., Bécard, G., and Roux, C. (2012) Comparative analysis of mitochondrial genomes of *Rhizophagus irregularis* - syn. *Glomus irregulare* - reveals a polymorphism induced by variability generating elements. *New Phytol* **196**: 1217–1227.
- Franco, M., López, S., Medina, R., Lucentini, C.G., Troncozo, M.I., Pastorino, G.N., et al. (2017) The mitochondrial genome of the plant-pathogenic fungus *Stemphylium lycopersici* uncovers a dynamic structure due to repetitive and mobile elements. *PLoS One* **12**: e0185545.
- Freel, K.C., Friedrich, A., Hou, J., and Schacherer, J. (2014) Population genomic analysis reveals highly conserved mitochondrial genomes in the yeast species *Lachancea thermotolerans*. *Genome Biol Evol* **6**: 2586–2594.
- Goodwin, S.B., McCorison, C.B., Cavaletto, J.R., Culley, D. E., LaButti, K., Baker, S.E., and Grigoriev, I.V. (2016) The mitochondrial genome of the ethanol-metabolizing, wine cellar mold *Zasmidium cellare* is the smallest for a filamentous ascomycete. *Fungal Biol* **120**: 961–974.
- Greiner, S., Lehwark, P., and Bock, R. (2019) OrganellarGenomeDRAW (OGDRAW) version 1.3.1: expanded toolkit for the graphical visualization of organellar genomes. *Nucleic Acids Res* **47**: W59–W64.
- Hall, T.A. (1999) BioEdit: a user-friendly biological sequence alignment editor and analysis program for windows 95/98/NT. *Nucleic Acids Symp Ser* **41**: 95–98.
- Hu, L., Zhang, M., Sun, Y., and Bu, Y. (2020) Characterization and phylogenetic analysis of the first complete mitochondrial genome of *Cylicocycclus radiatus*. *Vet Parasitol* **281**: 109097.
- Huang, C., and Liu, K. (2001) RAPD analysis of the pathogenic fungi of apple ring rot and other major related diseases. *Acta Phytopathol Sin* **31**: 69–74.
- Inderbitzin, P., Bostock, R.M., Trouillas, F.P., and Michailides, T.J. (2010) A six locus phylogeny reveals high species diversity in Botryosphaeriaceae from California almond. *Mycologia* **102**: 1350–1368.
- Johansen, S., and Haugen, P. (2001) A new nomenclature of group I introns in ribosomal DNA. *RNA* **7**: 935–936.
- Jung, P.P., Friedrich, A., Reisser, C., Hou, J., and Schacherer, J. (2012) Mitochondrial genome evolution in a single protoploid yeast species. *G3-Genes Genom Genet* **2**: 1103–1111.
- Katoh, K., and Standley, D.M. (2013) MAFFT multiple sequence alignment software version 7: improvements in performance and usability. *Mol Biol Evol* **30**: 772–780.
- Koganezawa, H., and Sakuma, T. (1984) Causal fungi of apple fruit rot. *Bull Fruit Tree Res Station C* **11**: 49–62.
- Kouvelis, V.N., Sialakouma, A., and Typas, M.A. (2008) Mitochondrial gene sequences alone or combined with ITS region sequences provide firm molecular criteria for

- the classification of *Lecanicillium* species. *Mycol Res* **112**: 829–844.
- Kumar, S., Stecher, G., and Tamura, K. (2016) MEGA7: molecular evolutionary genetics analysis version 7.0 for bigger datasets. *Mol Biol Evol* **33**: 1870–1874.
- Lang, B.F., Gray, M.W., and Burger, G. (1999) Mitochondrial genome evolution and the origin of eukaryotes. *Annu Rev Genet* **33**: 351–397.
- Lang, B.F., Laforest, M.J., and Burger, G. (2007) Mitochondrial introns: a critical view. *Trends Genet* **23**: 119–125.
- Li, Y., Qiu, Y.Y., Zeng, M.H., Diao, P.W., Chang, Q.C., Gao, Y., et al. (2019) The complete mitochondrial genome of *Echinostoma miyagawai*: comparisons with closely related species and phylogenetic implications. *Infect Genet Evol* **75**: 103961.
- Marsberg, A., Kemler, M., Jami, F., Nagel, J.H., Postma-Smidt, A., Naidoo, S., et al. (2017) *Botryosphaeria dothidea*: a latent pathogen of global importance to woody plant health. *Mol Plant Pathol* **18**: 477–488.
- McDonald, M.C., Taranto, A.P., Hill, E., Schwessinger, B., Liu, Z., Simpfendorfer, S., et al. (2019) Transposon-mediated horizontal transfer of the host-specific virulence protein ToxA between three fungal wheat pathogens. *mBio* **10**: e01515-19.
- Murray, M.G., and Thompson, W.F. (1980) Rapid isolation of high molecular weight plant DNA. *Nucleic Acids Res* **8**: 4321–4325.
- Ogata, T., Sano, T., and Harada, Y. (2000) *Botryosphaeria* spp. isolated from apple and several deciduous fruit trees are divided into three groups based on the production of warts on twigs, size of conidia, and nucleotide sequences of nuclear ribosomal DNA ITS regions. *Mycoscience* **41**: 331–337.
- Pantou, M.P., Kouvelis, V.N., and Typas, M.A. (2006) The complete mitochondrial genome of the vascular wilt fungus *Verticillium dahliae*: a novel gene order for *Verticillium* and a diagnostic tool for species identification. *Curr Genet* **50**: 125–136.
- Peng, B., Liu, L., Wu, H., Tian, L., Zhou, Z., and Gu, Q. (2011) The intraspecific genetic diversity of pathogenic fungi of apple ring rot. *Sci Agric Sin* **44**: 1125–1135 [in Chinese].
- Repar, J., and Warnecke, T. (2017) Mobile introns shape the genetic diversity of their host genes. *Genetics* **205**: 1641–1648.
- Ronquist, F., Teslenko, M., van der Mark, P., Ayres, D.L., Darling, A., Höhna, S., et al. (2012) MrBayes 3.2: efficient Bayesian phylogenetic inference and model choice across a large model space. *Syst Biol* **61**: 539–542.
- Rozas, J., Ferrer-Mata, A., Sánchez-DelBarrio, J.C., Guirao-Rico, S., Librado, P., Ramos-Onsins, S.E., and Sánchez-Gracia, A. (2017) DnaSP 6: DNA sequence polymorphism analysis of large data sets. *Mol Biol Evol* **34**: 3299–3302.
- Shen, X.Y., Li, T., Chen, S., Fan, L., Gao, J., and Hou, C.L. (2015) Characterization and phylogenetic analysis of the mitochondrial genome of *Shiraia bambusicola* reveals special features in the order of Pleosporales. *PLoS One* **10**: e0116466.
- Song, N., Geng, Y., and Li, X. (2020) The mitochondrial genome of the phytopathogenic fungus *Bipolaris sorokiniana* and the utility of mitochondrial genome to infer phylogeny of Dothideomycetes. *Front Microbiol* **11**: 863.
- Stamatakis, A. (2006) RAxML-VI-HPC: maximum likelihood-based phylogenetic analyses with thousands of taxa and mixed models. *Bioinformatics* **22**: 2688–2690.
- Stoddard, B.L. (2011) Homing endonucleases: from microbial genetic invaders to reagents for targeted DNA modification. *Structure* **19**: 7–15.
- Sun, G., and Zhang, T. (1996) A simple separation technique of single spore. *Plant Quarantine* **10**: 40–41 [in Chinese].
- Tang, W., Ding, Z., Zhou, Z., Wang, Y., and Guo, L. (2012) Phylogenetic and pathogenic analyses show that the causal agent of apple ring rot in China is *Botryosphaeria dothidea*. *Plant Dis* **96**: 486–496.
- Tillich, M., Lehwark, P., Pellizzer, T., Ulbricht-Jones, E.S., Fischer, A., Bock, R., and Greiner, S. (2017) GeSeq - versatile and accurate annotation of organelle genomes. *Nucleic Acids Res* **45**: W6–W11.
- Torriani, S.F., Goodwin, S.B., Kema, G.H., Pangilinan, J.L., and McDonald, B.A. (2008) Intraspecific comparison and annotation of two complete mitochondrial genome sequences from the plant pathogenic fungus *Mycosphaerella graminicola*. *Fungal Genet Biol* **45**: 628–637.
- Wang, B., Liang, X., Gleason, M.L., Zhang, R., and Sun, G. (2018a) Comparative genomics of *Botryosphaeria dothidea* and *B. kuwatsukai*, causal agents of apple ring rot, reveals both species expansion of pathogenicity-related genes and variations in virulence gene content during speciation. *IMA Fungus* **9**: 243–257.
- Wang, D., Zhang, Y., Zhang, Z., Zhu, J., and Yu, J. (2010) KaKs_Calculator 2.0: a toolkit incorporating gamma-series methods and sliding window strategies. *Genomics Proteomics Bioinformatics* **8**: 77–80.
- Wang, L., Zhang, S., Li, J.H., and Zhang, Y.J. (2018b) Mitochondrial genome, comparative analysis and evolutionary insights into the entomopathogenic fungus *Hirsutiella thompsonii*. *Environ Microbiol* **20**: 3393–3405.
- White, T.J., Bruns, T., Lee, S., and Taylor, J. (1990) Amplification and direct sequencing of fungal ribosomal RNA genes for phylogenetics. *PCR Protoc: Guide Methods Appl* **18**: 315–322.
- Xiao, S., Nguyen, D.T., Wu, B., and Hao, W. (2017) Genetic drift and indel mutation in the evolution of yeast mitochondrial genome size. *Genome Biol Evol* **9**: 3088–3099.
- Xu, C., Wang, C., Ju, L., Zhang, R., Biggs, A., Tanaka, E., et al. (2015) Multiple locus genealogies and phenotypic characters reappraise the causal agents of apple ring rot in China. *Fungal Divers* **71**: 215–231.
- Xu, C., Wang, C., Sun, X., Zhang, R., Gleason, M.L., Eiji, T., et al. (2013) Multiple group I introns in the small-subunit rDNA of *Botryosphaeria dothidea*: implication for intraspecific genetic diversity. *PLoS One* **8**: e67808.
- Yang, Y.Y., Li, S.N., Xu, L., Xing, Y.P., Zhao, R., Bao, G.H., et al. (2021) The complete mitochondrial genome of *Glycyrrhiza uralensis* Fisch. (Fabales, Leguminosae). *Mitochondrial DNA B* **6**: 475–477.
- Yu, Y., Harris, A.J., Blair, C., and He, X. (2015) RASP (reconstruct ancestral state in phylogenies): a tool for historical biogeography. *Mol Phylogenet Evol* **87**: 46–49.
- Zhang, S., and Zhang, Y.J. (2019) Proposal of a new nomenclature for introns in protein-coding genes in fungal mitogenomes. *IMA Fungus* **10**: 15.

Zhang, Z., Xiao, J., Wu, J., Zhang, H., Liu, G., Wang, X., and Dai, L. (2012) ParaAT: a parallel tool for constructing multiple protein-coding DNA alignments. *Biochem Biophys Res Commun* **419**: 779–781.

Supporting Information

Additional Supporting Information may be found in the online version of this article at the publisher's web-site:

Fig. S1. The ML phylogenetic tree of genus *Botryosphaeria* (Table S1) constructed using combined two genomic markers ITS and EF-1 α . Bootstrap percentages derived from 1000 replicates are indicated at the nodes. Bar = 0.01 substitutions per nucleotide position. The different colour and line sizes used were to distinguish overlapping areas (bootstrap 87 location). *Neofusicoccum luteum* was used as an outgroup.

Fig. S2. Comparison of mitogenome sizes between *B. dothidea* and *B. kuwatsukai* isolates. Significance difference was calculated of by t-test.

Fig. S3. Ratio of non-synonymous/synonymous (Ka/Ks) nucleotide substitutions. Ratios were calculated among the 12 protein-coding genes of the mitochondrial genome between *B. dothidea* and *B. kuwatsukai*.

Fig. S4. ML phylogenetic tree based on 12 concatenated mitochondrial core proteins (*cob-cox1-cox2-nad4L-nad5-atp6-nad1-nad4-nad6-cox3-nad2-nad3*). The tree

shown here was the single best topology recovered from ML by using RAxML software. Support values from ML analyses were given for nodes receiving strong supports. Bar = 0.02 substitutions per nucleotide position. *Zymoseptoria tritici* was used as an outgroup.

Table S1. GenBank accessions of four nuclear DNA markers of 17 isolates.

Table S2. Sizes and mitochondrial genome contents among selected species in the class Dothideomycetes (Orders Botryosphaerales, Capnodiales and Pleosporales).

Table S3. Comparison on nucleotide variations at exonic and intronic regions among different *B. dothidea* isolates.

Table S4. Co-conversion of exon sequences due to intron insertions.

Table S5. Comparison on nucleotide variations at exonic and intronic regions among different *B. kuwatsukai* isolates.

Table S6. Self-alignment results of intron nucleotide sequences of *B. dothidea* TCPTT1 using BLASTN.

Table S7. Alignment results of intron nucleotide sequences of *B. kuwatsukai* PGYT19 using BLASTN.

Table S8. Online BLAST results of introns identified in *B. dothidea* TCPTT1 mitogenome.

Table S9. Online BLAST results of introns identified in *B. kuwatsukai* PGYT19 mitogenome.

Table S10. Intron presence/absence patterns of the twelve *B. dothidea* isolates and five *B. kuwatsukai* isolates.